Coupled-oscillator model for hybridized optical phonon modes in contacting nanosize particles and quantum dot molecules

S. V. Koniakhin [1,*] O. I. Utesov [2,3,4] and A. G. Yashenkin [3,2]

[1]*Center for Theoretical Physics of Complex Systems, Institute for Basic Science, Daejeon 34126, Republic of Korea*
[2]*Department of Physics, St. Petersburg State University, St. Petersburg 199034, Russia*
[3]*Petersburg Nuclear Physics Institute NRC "Kurchatov Institute," Gatchina 188300, Russia*
[4]*St. Petersburg School of Physics, Mathematics, and Computer Science, HSE University, St. Petersburg 190008, Russia*

Modification of optical phonon spectra in contacting nonpolar nanoparticles compared to single particles is studied. Optical phonons in dielectric and semiconducting particles obey the Euclidean metric Klein-Fock-Gordon equation with Dirichlet boundary conditions. This equation is supposed to be solved numerically for manifolds of cojoined spheres. It is proposed to replace this problem with the simpler-to-solve coupled-oscillator model (COM), where an oscillator is attributed to each phonon mode of a particle and the particle overlap leads to the appearance of additional couplings for these oscillators with the magnitude proportional to the overlap volume. For not too big overlaps, this model describes solutions of the original eigenvalue problem with a quantitative level of accuracy. In particular, it works beyond isotropic s modes in dimers, which has been demonstrated for p modes in dimers and for tetramers. It is proposed to apply the COM for the description of recently manufactured dimer nanoparticles and quantum dots. The obtained results are in agreement with the dynamical matrix method for optical phonons in nanodiamonds. The dynamical matrix method is also used to demonstrate that the van der Waals contacts between faceted particles lead to very small modifications of the optical phonon spectra, which therefore could be neglected when discussing the propagation of vibrational excitations via a nanopowder. The possibility to distinguish between dimerized and size-distributed single particles from their Raman spectra is also considered. The proposed COM paves a way towards the description of propagation of vibrational modes in the ensembles of particles in contact including tight agglomerates, nanocrystal solids, and porous media.

I. INTRODUCTION

Raman spectroscopy is a powerful tool widely used for characterization of modern nanostructured materials including nanoparticles, nanorods, and two-dimensional nanostructures, which gives a precise energy fingerprint of the excitations peculiar to the material such as phonons [1–5], magnons [6–8], and excitons [9,10]. Currently, the Raman spectra measurements are the standard characterization procedure for carbon materials [11–13] and various application-oriented nanomaterials [14–22]. Combining the simplicity of implementation, the nondestructive nature, and versatile data obtained from spectra analysis, Raman spectroscopy contributes significantly to modern nanotechnology and materials science.

On the basic level, the structure of optical phonon lines obtained by Raman spectroscopy allows determination of the composition of a material. As far as nanoparticles are concerned, the more sophisticated theoretical approach applied to fit Raman spectra can yield many more parameters, i.e., the nanoparticle average size L, the deviation δL in the size distribution function, the concentration of lattice impurities, and the geometric shape (faceting) [23]. The nanoparticle size can be roughly estimated from the phonon confinement model (PCM) [16,24–29] or with higher accuracy (including the standard deviation in the size distribution) from the joint [30] dynamical matrix method [31]–bond polarization model (DMM-BPM) theory [32,33]. The nanoparticle shape (faceting) also affects the main peak position and overall peak structure [34] in Raman spectra of nanoparticles. Information about the type and the concentration of lattice impurities can be obtained from the broadening of the Raman peak for nanoparticles [23,35–37] and also for bulk materials [11,38–41]. This picture is actual for dielectric diamond nanoparticles as well as for crystalline Si, Ge, GaAs, and CdTe and many other types of semiconductor quantum dots.

Recently, promising objects such as quantum dot (QD) molecules have been synthesized and now they are a subject of extensive ongoing research [42–45]. Quantum dot dimers are investigated to find applications for biomolecule sensing and for nanoantennas with controlled polarization. An interesting feature that QD dimers demonstrate is their electronic

---

structure matching with that of molecules. Significant progress has been obtained in the fine control of the neck thickness, which gives a possibility to tune precisely the coupling constant between the monomers.

At the same time, the hybridization of optical phonons in nanoparticles in contact with each other and/or in QD dimers can affect the Raman spectrum of an ensemble and in particular the crystalline Raman peak shift and its shape. These effects are evidently important for characterization of the whole ensemble mentioned above.

In addition, a complete understanding of the optical phonon hybridization and of the coupling in QD molecules opens up the possibility to describe theoretically the role of interparticle contact in the Raman spectra of nanopowders, tight nanoparticle agglomerates [46,47], strongly coupled QD nanocrystal solids [48], and porous materials [49–53]. Currently, the Raman spectra analysis relies on the single-particle properties only. The present study addresses the problem of optical phonon modes in contacting and/or cojoined nanoparticles and quantum dots of nonpolar materials. We argue that along with direct calculation of these modes within the proposed geometry, the simple coupled-oscillator model (COM) could be used to qualitatively describe the corresponding vibrational spectra. After some insignificant improvements, the COM is sufficient to reproduce the principal features of optical phonon hybridization. This statement is verified using both continuous scalar Euclidean Klein-Fock-Gordon (EKFG) model (see Ref. [34]) and atomistic DMM approaches. In the strongly coupled regime of cojoined particles, the effect of hybridization on the Raman spectra is found to be pronounced, whereas in the case of weakly coupled (say, via the van der Waals forces) particles the corresponding optical phonon frequency shifts are negligible. The latter means that the theory of propagation of vibrational modes through a nanopowder can safely ignore the perturbations of phonon spectra in individual particles stemming from their contacts, operating only with the single-particle spectral characteristics.

Here it is pertinent to note that in polar materials there is a strong coupling between volume (and surface) phonons and the electromagnetic field, which results in shape-dependent shifts itself (see, e.g., Refs. [54–56]). A corresponding theory for dimerized systems is an interesting and important problem. In the case of nonpolar materials, the physics behind the COM is quite simple: We have well-defined vibrational modes in each of the particles, which interact only through the intersection volume. Next they hybridize in accordance with COM predictions in both strongly coupled (resonance) and weakly coupled (out-of-resonance) regimes. The main advantage of the COM is directly connected to its computational simplicity. This concerns the possibility to build up a semimicroscopic theory of interparticle vibrational modes propagating in a granular medium.

Importantly, we show that the usual tunneling tight-binding model for the Schrödinger equation (see, e.g., Ref. [57]) is not applicable for our problem. It makes incorrect predictions for the hybridized phonon frequencies even on the quantitative level.

The rest of the paper is organized as follows. In Sec. II we start with a description of the model of coupled oscillators
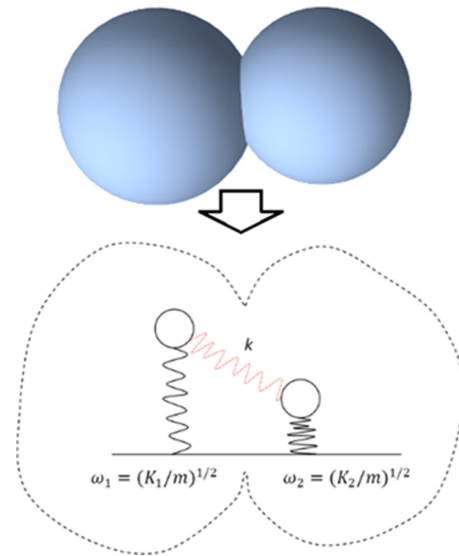

FIG. 1. Eigenvalue problem of the Laplace operator $\Delta \psi + q^2 \psi = 0$ with Dirichlet boundary conditions $\psi|_{\partial \Omega} = 0$ on the manifold of two cojoined spheres has solutions close to the model of two coupled harmonic oscillators.

to familiarize readers with the approach to be developed. Then we utilize the EKFG model for insight into the problem of optical phonons in the cojoined spherical particles. We demonstrate the similarity of these problems and build up consistent perturbation theory formulating the COM for eigenvalues and eigenfunctions of intersecting spheres. In Sec. III we use the microscopic DMM model and compare its predictions with the yield of the EKFG and coupled-oscillator approaches. We also use the DMM-BPM approach to study the case of two faceted particles in contact through weak van der Waals interaction. In Sec. IV we study the effect of nanoparticle dimerization on the Raman spectra. Section V discusses our results. We summarize in Sec. VI.

II. SEMIQUANTITATIVE APPROACH: COUPLED OSCILLATORS AND EKFG THEORY

Below we show that there is a good correspondence between the eigenmodes of the EKFG approach for cojoined particles and the classical problem of two coupled oscillators (COM; see Fig. 1).

A. Coupled oscillators

The Lagrange function of two coupled oscillators reads

$$\mathcal{L} = \frac{m\dot{x}_1^2}{2} + \frac{m\dot{x}_2^2}{2} - \frac{k_1 x_1^2}{2} - \frac{k_2 x_2^2}{2} - \frac{k_{\text{int}}(x_1 - x_2)^2}{2}, \quad (1)$$

where two oscillators with frequencies $\omega_{1,2}^2 = k_{1,2}/m$ are assumed to be coupled by the spring with rigidity k_{int}. Newtonian equations of motion can be written as

$$m\ddot{x}_1 = -k_1 x_1 - k_{\text{int}}(x_1 - x_2),$$
$$m\ddot{x}_2 = -k_2 x_2 - k_{\text{int}}(x_2 - x_1). \quad (2)$$

To find the harmonic solutions, we rewrite them as

$$(k_1 + k_{\text{int}})x_1 - k_{\text{int}}x_2 = m\omega^2 x_1,$$
$$(k_2 + k_{\text{int}})x_2 - k_{\text{int}}x_1 = m\omega^2 x_2. \tag{3}$$

The eigenvalues (squares of frequencies) are given by

$$\omega_\pm^2 = \frac{k_1 + k_2 + 2k_{\text{int}} \pm \sqrt{(k_1 - k_2)^2 + 4k_{\text{int}}^2}}{2m}. \tag{4}$$

In the particular resonant case $k_1 = k_2 = k$ we have

$$\omega_+^2 = \frac{k + 2k_{\text{int}}}{m}, \quad \omega_-^2 = \frac{k}{m} \tag{5}$$

for $x_1 - x_2$ and $x_1 + x_2$ eigenfunctions, respectively. We see that one resonant solution is not affected by the coupling, whereas the frequency of the other one increases linearly with the parameter k_{int}. In the highly off-resonant case $|k_1 - k_2| \gg k_{\text{int}}$ we get

$$\omega_\pm^2 = \frac{k_{1,2} + k_{\text{int}}}{m}, \tag{6}$$

so the oscillators almost do not "feel" each other, but they feel the additional spring.

We discuss the two oscillators case above. However, we note that the generalization for $n > 2$ coupled-oscillator problem is straightforward.

B. The EKFG model

The continuous method of finding the eigenfunctions and the eigenvalues of the long-wavelength optical phonon modes applicable for the *arbitrary* shape of the manifold Ω starts from evaluation of the Euclidean metric Klein-Fock-Gordon equation [34]

$$\left(\partial_t^2 + C_1 \Delta + C_2\right)\psi = 0, \quad \psi|_{\partial\Omega} = 0, \tag{7}$$

where ψ is an envelope function of the optical vibration, which indicates the amplitude of the relative displacements of neighboring atoms, and the second expression refers to the Dirichlet boundary conditions. The parameters $C_{1,2}$ are related to the constants of the optical phonon dispersion in the long-wavelength limit via

$$\omega^2 = C_2 - C_1 q^2 \iff \omega(q) \approx \sqrt{C_2} - \frac{C_1}{\sqrt{C_2}}\frac{q^2}{2} \equiv \omega_0 - \alpha q^2, \tag{8}$$

where ω_0 is the maximal optical mode frequency and q^2 is the eigenvalue of the corresponding boundary value problem

$$\Delta\psi + q^2\psi = 0, \quad \psi|_{\partial\Omega} = 0. \tag{9}$$

This equation can be solved numerically for an arbitrary manifold using, e.g., Wolfram *Mathematica*. We dub ψ a wave function.

Unlike the yield of the PCM, the realistic structure of the phonon spectrum in nanoparticles is discrete like in diamondoids [58,59] and in fullerenes [32]. The vibrational modes should resemble the standing-wave-like eigenmodes of a resonator of the same shape as the nanoparticle or, more generally, electron orbitals in an atom (see Refs. [30,34]). Therefore, their classification into *s*, *p*, etc., orbital-like classes makes perfect sense, at least for spherical particles and
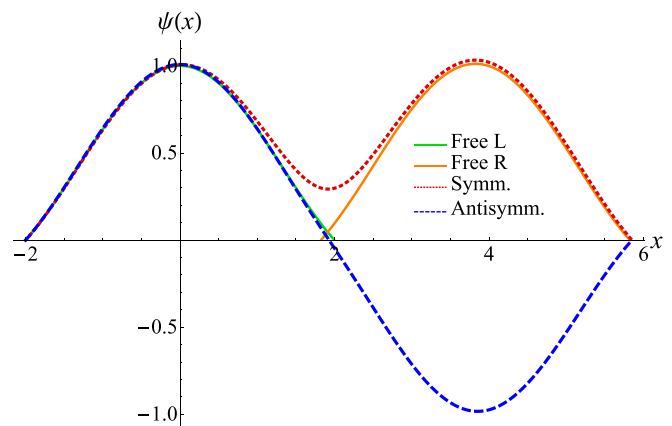

FIG. 2. Phonon wave functions of *s* modes along the *x* axis (connecting the centers) for noncontacting spheres with radii $R_1 = R_2 = 2$ (green and orange, manually shifted left by δr, the eigenvalues $q_1^2 = q_2^2 = 2.469$) and for symmetric and antisymmetric modes of the dimer with $\delta r = 0.2$ (red and blue, eigenvalues $q^2 = 2.447, 2.471$). The antisymmetric mode is very close to the mode of the free particles and has nearly the same eigenvalue. The eigenvalue of the symmetric mode is strongly shifted and the wave function profile differs, in particular in the contact region. The symmetric mode in the spheres corresponds to the antisymmetric mode in the coupled-oscillator approach.

their cojoined combinations. In particular, this means that the formation of the symmetric (bonding) and the antisymmetric (antibonding) states in nanoparticle dimers (or quantum dot molecules) should occur on the same footing as in real atoms and molecules.

Figure 2 shows optical phonon wave functions with smallest q^2 in two cojoined spheres with radii $R_1 = R_2 = 2$ and the penetration length $\delta r = 0.2$ (all the distances are measured in the lattice parameter a_0 units unless specified otherwise). It is important to underscore that the antisymmetric eigenfunction profile nearly coincides with the wave function profile of an isolated sphere. The eigenvalue of the antisymmetric mode is also very close to the one of the isolated sphere. In contrast, the symmetric wave function differs significantly from the isolated sphere wave function in the region of contact. The eigenvalue, corresponding to this function, is also downshifted with respect to the isolated sphere eigenvalue.

Figure 3 shows the two smallest eigenvalues for two interpenetrated spheres as a function of penetration length δr [Fig. 3(a)] and as a function of the radius of one of the spheres R_2 [Fig. 3(b)]. The fit with the use of eigenvalues of the coupled-oscillator Hamiltonian (discussed below) is also depicted. One can see the avoided crossing behavior of the eigenvalues, which is captured by both the EKFG model and the COM. However, in contrast to the tunneling Jaynes-Cummings Hamiltonian [60], both eigenvalues are downshifted. The latter is typical for the COM and will be discussed in more detail below. The crucial parameter for the developed theory is the intersection volume of two particles in the dimer, which is quadratic in penetration length δr under the assumption that $\delta r \ll R_{1,2}$:

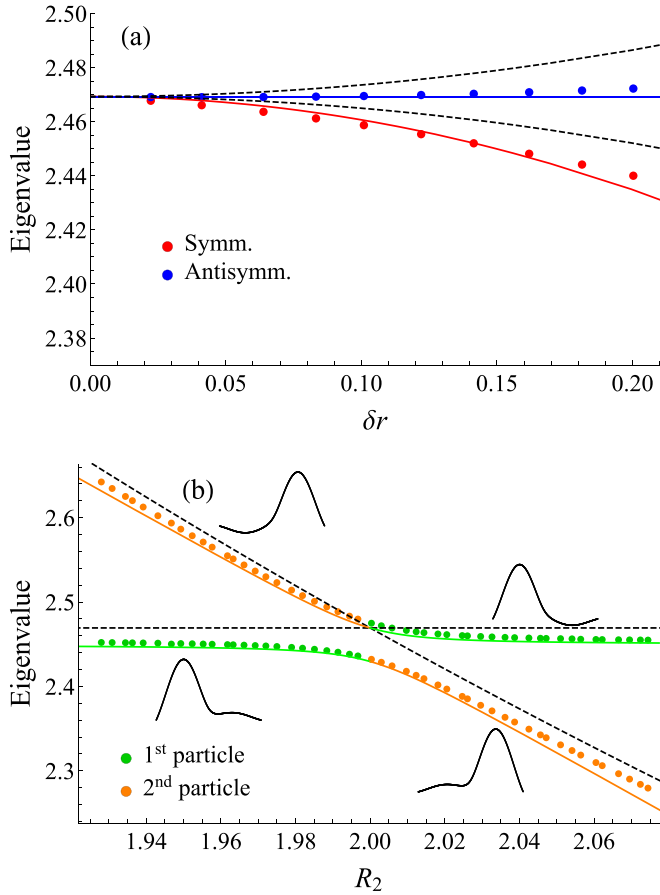$$V_{12}(R_1, R_2, \delta r) \approx \frac{\pi \delta r^2 R_1 R_2}{R_1 + R_2} + O(\delta r^3). \tag{10}$$

FIG. 3. (a) Two smallest eigenvalues of the Laplace operator in the system of two spheres of radii 2 as a function of penetration length δr represented by red (symmetrical ψ) and blue (antisymmetrical ψ) markers. Blue and red curves show the result of the coupled-oscillator approach [see Eq. (4)] for $k_1 = k_2$ and black dashed curves show the result of the tunneling tight-binding model without the on-site corrections. The dependence $k_{\mathrm{int}} \propto \delta r^2$ is used. (b) Two upper Laplacian eigenvalues in the system of the two spheres with fixed penetration length $\delta r = 0.21$ and the radius of the left particle $R_1 = 2$ as a function of the right particle radius R_2. The green points correspond to the eigenfunctions concentrated in the first particle and the orange ones correspond to the eigenfunctions with domination inside the second particle. The orange and green solid curves represent the fit with the use of Eq. (4) for fixed k_1 and k_{int} and $k_2 = k_1 + \mathrm{const}(R_2 - 2)$. Freestanding black curves show the sketched shapes of the wave functions. Dashed lines are for the eigenvalues of isolated particles.

C. How to construct the coupled-oscillator Hamiltonian

Basing on the results presented above, now we formulate the following rules allowing one to construct the Hamiltonian of the coupled-oscillator model H_{pq} capable of reproducing the optical phonon modes in contacting particles. The indices p and q in H span all the modes of interest in all the particles considered (more than two of them may exist), e.g., $p \rightarrow (i, m)$ stands for the mth mode in the ith particle.

(i) For each pair of particles i and j one calculates the intersection (overlap) volume V_{ij}. Either its approximate value given by Eq. (10) or precise value could be taken.

(ii) For each mode m of interest in the ith particle one writes in the diagonal element H_{pp} of the Hamiltonian [where $p = (i, m)$] its bare eigenvalue q_{im}^2. For optical phonons it should be taken as the value of the size-quantization induced redshift of the given mode frequency in the ith nanoparticle with respect to its bulk crystal value ω_0 measured in units of cm^{-1} [see Eq. (8)].

(iii) For each mode m one calculates the on-site volume correction (diagonal) by summing over the neighboring particles j: $\Delta_p \equiv \Delta_{im} = q_{im}^2 \alpha_m \sum_j f(V_{ij}/V_i)$. After that, one adds the result to the diagonal matrix element. The factor α_m (discussed below) depends on the symmetry of the modes s, p, etc., $f(x) = x - (x/0.425)^2$, where the second term is an empirical correction important for relatively large penetrations.

(iv) For each pair of modes from different particles one calculates the off-diagonal coupling terms $H_{pq} = -C_{pq} = -\sqrt{q_{im}^2 q_{jn}^2} \beta_{mn} V_{ij}/\sqrt{V_i V_j}$. Here again β_{mn} are the coefficients, dependent on the symmetry of the modes (discussed below).

(v) The eigenvalues of H should be subtracted from ω_0 in order to obtain the physical frequencies visible in the Raman spectra. The eigenfunctions of H reveal the amplitudes of phonon modes located at the particles under consideration.

It is pertinent to note that one can (and should) consider only several close in energy modes; the effect of further modes (including acoustic) is negligible.

D. Examples of construction

According to this construction algorithm, the dimension of H is the number of all modes in all particles. If we are interested in, say, only the lowest s modes, it reduces to the number of particles N. If one s and three p modes at each particle are considered, then the dimension of H will be $4N$, etc. The shape-dependent coefficients are $\alpha_s = 1$, $\alpha_p = 3$, $\beta_{ss} = 1$, $\beta_{sp} = 3$, and $\beta_{pp} = 4.5$.

For the simplest case of two particles and accounting for s modes only (thus the mode indices m and n could be omitted), the coupled-oscillator Hamiltonian reads

$$H = \begin{pmatrix} q_1^2 - \Delta_1 & -C_{12} \\ -C_{12} & q_2^2 - \Delta_2 \end{pmatrix}. \tag{11}$$

In the case of identical particles and small penetrations [$f(x) = x$], the on-site corrections and couplings are equal to each other $\Delta_1 = \Delta_2 = C_{12}$ and the Hamiltonian essentially coincides with the eigenvalue problem for two coupled oscillators given by Eq. (3). The only difference is the negative sign in front of k_{int} on the diagonal. As a result, in the resonant case, the COM eigenvalue that corresponds to the antisymmetric eigenfunction $(1, -1)^T$ does not change (cf. Fig. 2), whereas for real coupled harmonic oscillators [Eq. (3)] it holds for the symmetric eigenfunction. The second eigenvalue, which is lower in magnitude, corresponds in the COM to the symmetric wave function $(1, 1)^T$, while for real coupled harmonic oscillators this eigenvalue with changed

(higher) magnitude is related to the antisymmetric wave function.

In is instructive to compare the obtained Hamiltonian with the one obtained using the quantum-mechanical tight-binding model (TBM) [61] for the case of coupled quantum wells. First, both of them contain the additional terms on the diagonals and the off-diagonal coupling terms [cf. Eq. (11) above and Eqs. (24) and (25) in Ref. [57]]. However, the diagonal terms for the TBM are generally much smaller than the off-diagonal ones according to Eq. (14) from Ref. [57]. As a result, the levels split nearly symmetrically with respect to their initial position [see Eqs. (53) and (54) in Ref. [57]], giving as a limit the famous Jaynes-Cummings Hamiltonian [60], applicable for variety of two-level systems:

$$H = \begin{pmatrix} k_1 & k_{\text{int}} \\ k_{\text{int}} & k_2 \end{pmatrix}. \tag{12}$$

In contrast, within the framework of the COM, the antisymmetric state has the same energy as the initial energy levels, while the symmetric state is shifted. The splitting itself in both the COM and the TBM equals approximately twice the off-diagonal terms. The obvious similarity is in the emergence of symmetric and antisymmetric states both in continuous approaches (cf. Fig. 2 above versus Fig. 5 from Ref. [57]) and in spinor form [see Eq. (57) in Ref. [57]]. Furthermore, if one directly applies the algorithm of the matrix element calculation from Ref. [57], one should treat zero boundary conditions as an infinite potential, presuming explicitly zero matrix elements.

When considering the case of unequal spheres, an additional difference appears. The on-site volume correction terms depend only on the intersection volume, the sphere volume, and the bare eigenvalue of this sphere. Physically, this means that an additional volume in the neighboring particle becomes accessible for the phonon mode from the first nanoparticle. This volume does not depend on the precise shape of the second overlapped manifold. The coupling term is in fact the geometrical mean of the on-site volume corrections [within the assumption $f(x) = x$], which is equal to the on-site volume correction only for equal spheres.

For the more complicated case of two particles with two modes ($m, n = 1$ for s and $m, n = 2$ for the p_x mode) at each
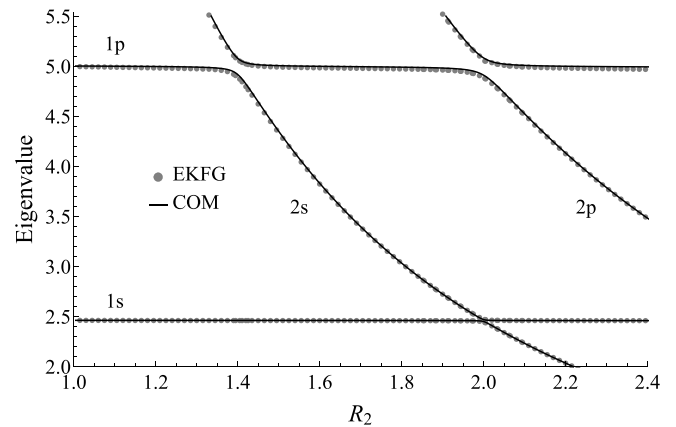

FIG. 4. Four highest eigenvalues for the nanoparticle dimer when varying the size of the second particle while keeping constant the size of the first one and the penetration length ($R_1 = 2$ and $\delta r_{12} = 0.2$). The dots show the solution of the full Dirichlet eigenvalue problem $\Delta \psi + q^2 \psi = 0$. The curves show the results of the coupled-oscillator model.

particle, we have the Hamiltonian

$$H = \begin{pmatrix} q_1^2 - \Delta_1 & 0 & -C_{13} & -C_{14} \\ 0 & q_2^2 - \Delta_2 & -C_{23} & -C_{24} \\ -C_{13} & -C_{23} & q_3^2 - \Delta_3 & 0 \\ -C_{14} & -C_{24} & 0 & q_4^2 - \Delta_4 \end{pmatrix}, \tag{13}$$

where the notation $p \to (i, m)$ has the explicit form $1 \to (1, 1)$, $2 \to (1, 2)$, $3 \to (2, 1)$, and $4 \to (2, 2)$. Among the p modes, only those aligned along the x axis are considered because p_y and p_z modes have vanishing overlaps at small penetrations.

Figure 4 shows the result of diagonalization together with the results of the EKFG numerical calculation of the Laplace eigenvalue problem. Once again, one can see good agreement between the exact solution and the coupled-oscillator approach.

Finally, we check the applicability of our approach to an important case of many particles in contact. We consider only s modes in four identical particles located at the vertices of a slightly deformed square, which form a tetramer. The corresponding Hamiltonian for small penetrations [$f(x) = x$] has the form

$$H = \begin{pmatrix} q^2 - C_{12} - C_{13} & -C_{12} & -C_{13} & 0 \\ -C_{12} & q^2 - C_{12} - C_{24} & 0 & -C_{24} \\ -C_{13} & 0 & q^2 - C_{13} - C_{34} & -C_{34} \\ 0 & -C_{24} & -C_{34} & q^2 - C_{24} - C_{34} \end{pmatrix}. \tag{14}$$

The on-site volume correction terms Δ_i are here written explicitly via the couplings $C_{ij} = q^2 V_{ij}/V$ to underscore the contributions of two neighbors for each particle. The mode indices are omitted, similar to Eq. (11).

In order to investigate an even more complicated case, we study numerically unequal spheres with the Hamiltonian (14)

modified according to the rules formulated in the preceding section. Figure 5 shows the result of diagonalization for the Hamiltonian constructed within the coupled-oscillator model and the results of the numerical solution of the eigenvalue problem for the Laplace operator with Dirichlet boundary conditions. One sees a very good correspondence between
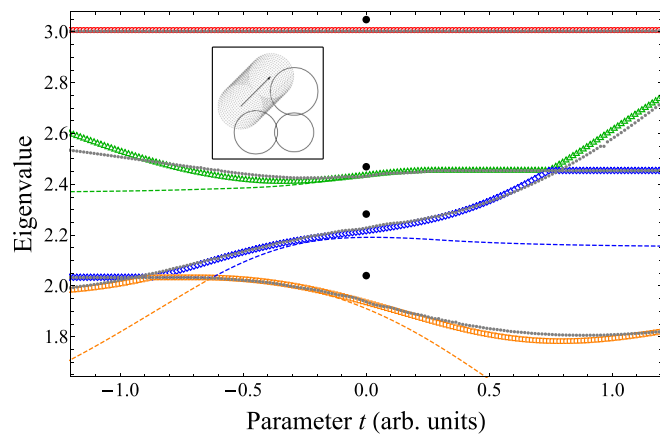
FIG. 5. Four lowest eigenvalues for various configurations of a tetramer. Initially, four particles with radii 2, 1.8, 2.2, and 2.08 are placed in the corners of a rectangle in the XY plane. The sides of the rectangle could be calculated from the penetration lengths $\delta r_{12} = 0.26$ and $\delta r_{23} = 0.22$. Then the fourth particle is moved by t along the horizontal and vertical axes. The trajectory of the center is depicted by an arrow in the inset, which gives the top view. The gray dots represent the results for the original Dirichlet eigenvalue problem $\Delta\psi + q^2\psi = 0$. The colored dashed curves are for the 4×4 H for s modes with $f(x) = x$ and approximate intersection volumes V_{ij} calculation via Eq. (10). The colored open markers are for the 4×4 H for s modes with $f(x) = x - (x/0.425)^2$ and precise calculation of the intersection volumes.

the approaches. Only at very high penetration lengths do the deviations become significant.

III. DYNAMICAL MATRIX METHOD

The more direct atomistic DMM of the treatment of optical phonons is even better adapted for precise calculations of vibrational modes in nanoparticles including the intermediate-wavelength regime and phonon polarizations. It also allows us to consider the loose arrays of faceted nanoparticles weakly interacting via the van der Waals forces.

A. Method formulation

The DMM is successful in obtaining the vibrational modes of molecules, atomic clusters, and nanoparticles. It is based on writing Newton's second law for all atoms with the forces caused by bonds stretching and bending of valence angles. Incorporating into calculations the conventional Keating model [62–65] allows us to write these equations of motion in the form

$$m\ddot{r}_p = M_{pq}r_q, \tag{15}$$

with the designations $p = (i, \alpha)$ and $q = (j, \beta)$, where latin letters enumerate the atoms and greek letters span over the Cartesian coordinates $\alpha, \beta = x, y, z$. The dynamical matrix is given by

$$M_{pq} = \sum_{j=1}^{N} \sum_{\beta=x,y,z} \frac{\partial^2 \Phi(\mathbf{r}_1, \mathbf{r}_2, \ldots)}{\partial r_{j,\alpha} \partial r_{j,\beta}} r_{j,\beta}. \tag{16}$$

In Eqs. (15) and (16) m is the mass assumed to be the same for all atoms and Φ is the total potential energy of nanocrystallites expressed via displacements $\mathbf{r}_i$ of atoms from their equilibrium positions. More specifically, Φ is a sum of pairwise interaction energies for bond stretching and depends on the positions of three atoms for valence angles deformations.

Equation (15) can be solved to trace the time dynamics from some initial conditions or, in the frequency representation, to obtain the phonon frequencies and eigenmodes:

$$m\omega^2 r_p = -M_{pq}r_q. \tag{17}$$

The vector r_p contains all information about phases and directions of atomic displacements.

B. Results for conjoined spheres: Comparison with the COM

It is natural to verify the proposed coupled-oscillator model by a comparison of its predictions with the numerical results of the atomistic DMM. When constructing the coupled-oscillator Hamiltonian using Eq. (11), one can directly take the Dirichlet problem bare eigenvalue q^2 for separate particle as its energy redshift $q^2 = \omega_0 - \omega$ with respect to the optical phonon frequency in the Brillouin zone center ω_0 [see Eq. (8); here we set $\alpha = 1$ and measure q^2 in cm^{-1}]. Note that below we will discuss the results in terms of the optical phonon frequencies taking the diamond with $\omega_0 = 1333$ cm^{-1} as an example. We choose the Keating model parameters as in Ref. [30].

Figure 6 shows the six highest eigenvalues for a couple of diamond particles as a function of penetration length δr obtained using the DMM approach (the lowest eigenvalues q^2 of the Dirichlet problem in terms of the EKFG approach due to the dispersion law with negative effective mass). The obtained data are compared with the predictions of the COM. One sees that for various optical phonon polarizations the
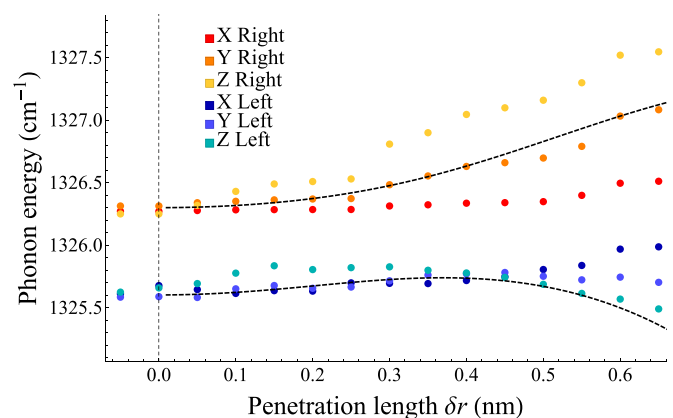

FIG. 6. Six highest phonon frequencies of 2.4- and 2.3-nm spherical diamond particles in contact as a function of penetration length δr. Different colors correspond to various phonon polarizations. Red, orange, and yellow are for eigenfunctions mainly localized inside the 2.4-nm particle (right particle). Blue tones correspond to the 2.3-nm particle (left particle). The dashed curve is obtained based on the coupled-oscillator model.
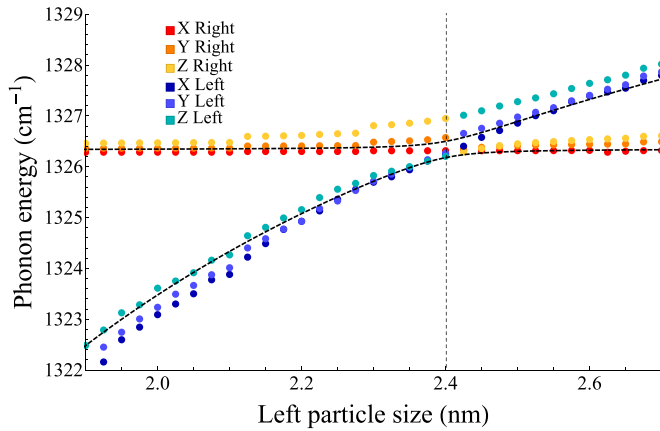
FIG. 7. Six highest phonon frequencies of the nanoparticle dimer as a function of the diameter of the second (left) particle. The size of the right particle is 2.4 nm. The dashed curves are obtained based on the coupled-oscillator model.

couplings have differing magnitudes. Still, the COM works semiquantitatively. The out-of-resonance case similar to what we expect from Eq. (6) is visible at small penetrations where both energies are shifted equally and the shift is proportional to δr^2.

One sees that polarization results in more complicated behavior of modes hybridization. The COM describes the situation for all separate modes qualitatively and for their sum quantitatively. Figure 7 illustrates the same idea, investigating the case when we vary the size of one of the particles while the penetration length remains intact.

C. Results for weakly interacting faceted particles

Another important and physically meaningful case is attaching of faceted particles. The underlying mechanism of their interaction can be the van der Waals forces or the covalent ones similar to the dimer case. Below we use k for the rigidities of interparticle bonds and K for the regular intraparticle (covalent) ones.

Figure 8 shows the frequency shifts of the three highest phonon modes in each cubic particle of a touching couple. The sizes of particles are 1.8 and 1.7 nm, respectively. For $k/K \ll 1$ the frequencies are all blueshifted linearly with the bond strength k, which qualitatively corresponds to the out-of-resonance case. Physically, the van der Waals interaction constant k is about three orders of magnitude lower than the covalent one [64,66].

One can estimate the coupling-induced frequency shift as $\delta\omega \propto \omega_0 \psi_{\text{surf}}^2 V_{\text{inter}}(k/K)$, where ψ_{surf} is an estimation of the atomic displacements magnitude at the surface and $V = Sa_0$ is the effective interaction volume (S is the contact surface and a_0 is the lattice parameter):

$$\delta\omega = \text{const} \times \omega_0 \left(\frac{1}{\sqrt{L^3}} \times \frac{a_0}{L}\right)^2 \times (a_0 S) \times \frac{k}{K}. \quad (18)$$

For the case of faceted particles whose facet surface and therefore contact area are proportional to the size L, the following
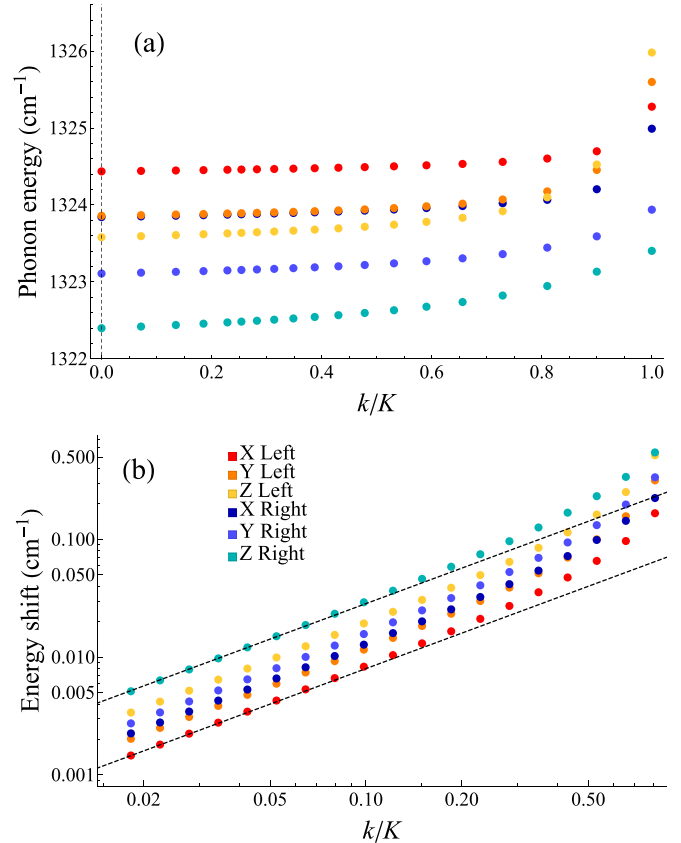

FIG. 8. (a) Energies of six highest phonon modes for two weakly interacting cubic particles of sizes 1.9 and 1.8 nm as functions of the ratio k/K. (b) Same as (a) but for energy shifts with respect to the $k = 0$ case (noninteracting particles). Guides to the eye for linear dependences are given.

scaling takes place:

$$\delta\omega = \text{const} \times \omega_0 \times s_{\text{rel}} \left(\frac{a_0}{L}\right)^3 \times \frac{k}{K}. \quad (19)$$

Here $s_{\text{rel}} = s/S$ is the percentage of surface experiencing contact with the neighboring particle.

In Fig. 9 one can see the shift saturation occurring because the phonon wave function (the standing wave in the shape of the product of three cosine functions for cubes) decreases from the facet center to its edges. As a result, the overlap of the wave functions of two particles is defined by the central regions of the facets. In practice, the effects should be even smaller because of a mismatch between contacting facets, their corrugations, and the presence of functional groups. We conclude that without a big spot of covalent bonds, the effect of contacts on optical phonons in general and on Raman spectra in particular is negligible taking into account the present accuracy of measurements. From the point of view of the possibility to build up an adequate theory of modes propagating in such a medium, this implies that one can use for this purpose the unperturbed eigenfunctions and eigenvalues of isolated particles.
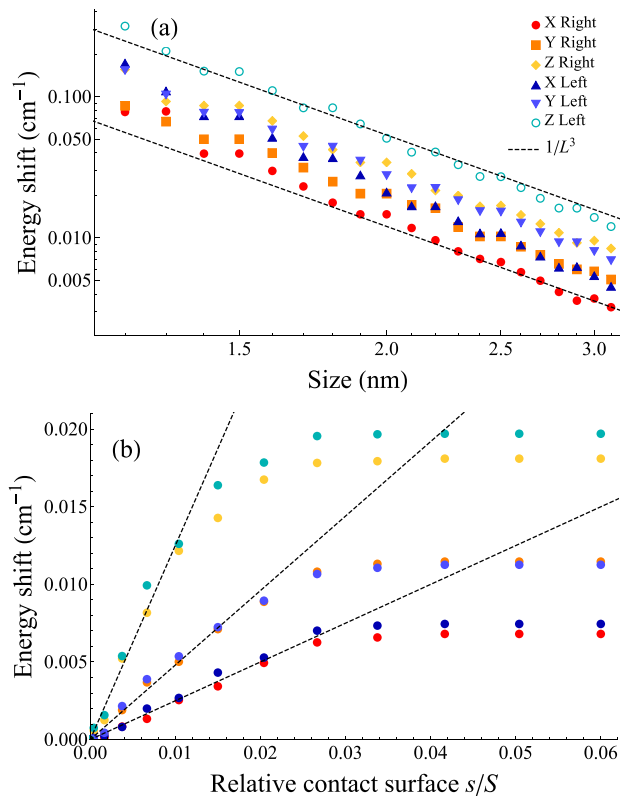
FIG. 9. (a) Energy shifts of the six highest phonon modes for two cubic particles of size L (given by the horizontal axis) and $0.9L$ in contact; the ratio k/K is 0.2. Shifts are calculated with respect to the noninteracting particles $k/K = 0$. The dashed lines are guides to the eye for the L^{-3} power law. (b) Eigenvalue shift as a function of contact surface s with respect to the full surface $s/S = l^2/6L^2$. Two equal 3-nm cubes are in contact only in the central square-shaped region (of size $l < L$) of their joint facet; the bond strengths in contact are $k/K = 0.333$. For a large range of parameters the energy shift is linear in s/S; the corresponding guides to the eye are depicted.

IV. APPLICATION OF THE COM FOR RAMAN SPECTRUM CALCULATION

In this section we study the effect of nanoparticle dimerization on the Raman spectra. Silicon nanoparticles with a mean size of 4 nm are normally distributed around this value (with a FWHM of 5% of the mean value). The corresponding Raman spectra [27,28,67–69] are redshifted by approximately 5 cm^{-1} with respect to the bulk silicon with the peak centered at 520 cm^{-1}. The nanoparticle dimers with penetration length distributed uniformly in the range from 0 to 1 nm are compared with the aforementioned case. Within the EKFG model, the spectra are calculated using the standard procedure [34] formulated as follows. The intensity of each mode is given by the square of the wave function volume integral $|\int \psi(\mathbf{r})d\mathbf{r}|^2$ (cf. with the structure factor in the conventional scattering problems for $q = 0$) and then the summation over all modes is performed in order to incorporate the phonon peak intensities and their positions into the Raman peak. The Raman spectrum can be also obtained using the COM. Within the isotropic s-mode approximation resulting in the 2×2 Hamiltonian for the dimer, the intensity of each of the two modes is
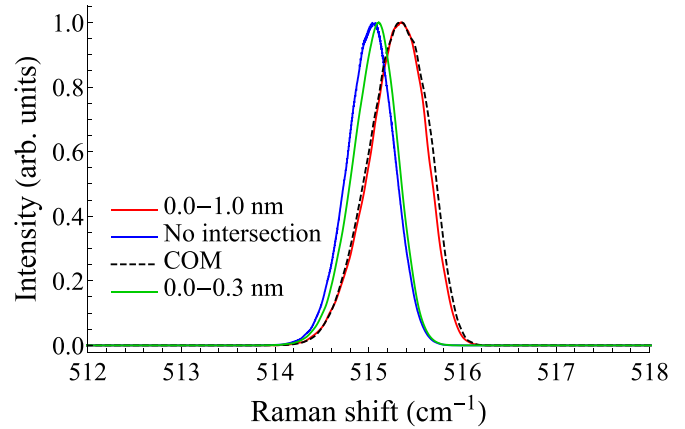

FIG. 10. Raman spectra of (4 ± 0.1)-nm silicon particles with and without (blue curve) dimerization. Red curve gives the EKFG approach yield for penetration lengths varying randomly from 0 to 1 nm. The black dashed curve is for the Raman spectrum obtained using the coupled-oscillator approach with the same size and penetration length distributions. The green solid curve is for smaller penetration lengths from 0 to 0.3 nm.

proportional to $|\psi_1 V_1 + \psi_2 V_2|^2$, where ψ_i stands for the components of the spinor ψ. Figure 10 shows the Raman spectra of free particles and nanoparticle dimers.

One sees the full agreement between the EKFG model and the COM. Dimerization results in a decrease of the redshift of the peak and in a change of its shape. Effectively, it can be explained by a higher volume accessible for the phonons which suppresses the confinement and reduces the size quantization effects. The effect of dimerization is at the level of experimental accuracy of modern spectrometers (0.3 cm^{-1}); however, the peaks differ significantly in their shape. The peak asymmetry coefficient for dimers is 0.37 whereas for free particles it is 0.22, which in our opinion rules out the possibility of confusion. We believe that incorporating into the theory the out-of-shell effects [35], making the phonon lines even more asymmetric, will further improve the situation.

As it was shown above, the COM approach can be adjusted to the case of many ($n > 2$) particles. Calculation of Raman spectra from the those obtained by the COM eigenstates for $n > 2$ can be scaled as well, in the same manner as for the above-described case of spinor (two-component) eigenstates for dimerized particles. Figure 11 shows Raman spectra for regular arrays (particles arranged in simple cubic lattice) of various sizes calculated using both the DMM-BPM and COM approaches. Importantly, due to atomic effects on the surface, the particles in clusters are not equal and experience slight scatter in the number of atoms, which can be accounted for as scatter in size in the framework of the COM. Three polarizations are also slightly split due to lowering the symmetry. Finally, the coupling constants (the off-diagonal terms) fluctuate for various polarizations, as can be seen in Figs. 6 and 7. All this requires averaging over relative orientations between particles in array and crystallographic directions when using the DMM-BPM approach and providing the equivalent averaging over nanoparticle sizes and values of coupling constants when using the COM. For 2.4-nm particles, the latter is
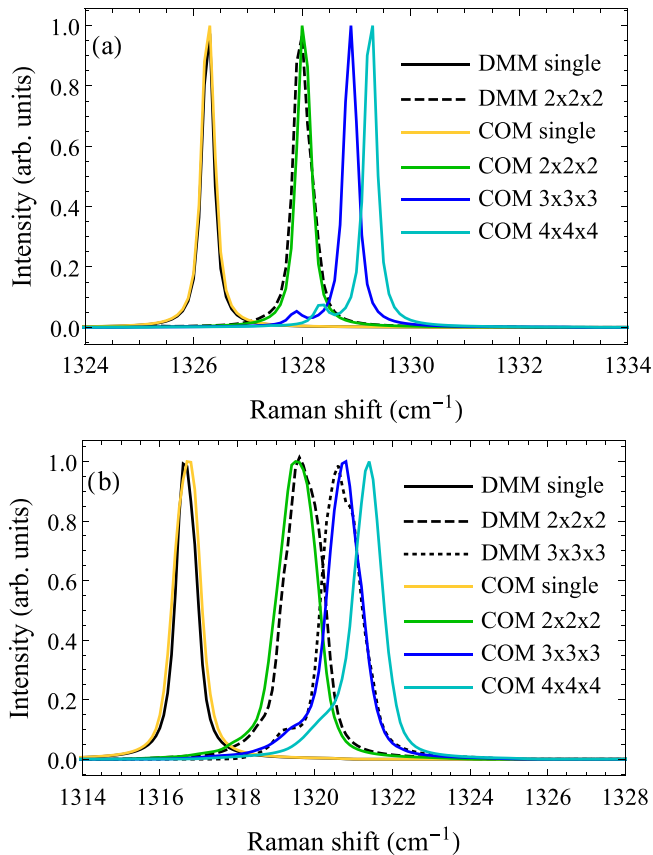
FIG. 11. (a) Raman spectra of regular arrays of diamond nanoparticles of size $L = 2.4$ nm and penetration length $\delta R = 0.2L$. A comparison of the DMM and COM is given for a single particle and a $2 \times 2 \times 2$ array. Fully atomistic DMM models contain approximately 1300 and 10 000 atoms, respectively. Arrays of larger sizes can be treated only using the COM approach. (b) Same as (a) but for lower nanoparticle size $L = 1.6$ nm and $\delta R = 0.15L$, which allows calculation of the $3 \times 3 \times 3$ array using the the DMM-BPM approach.

characterized by a 0.005 coefficient of variation in nanoparticle size distribution and 0.13 for the coefficient of variation in distribution of coupling constants. For 1.6-nm particles, the coefficients of variation are larger and have the values 0.01 and 0.5, respectively. One sees good agreement of the DMM-BPM and COM approaches when calculating Raman spectra of many-particle arrays. Importantly, the COM approach allows calculating Raman spectra for the systems inaccessible by the fully atomistic DMM-BPM approach. Thus the application of the COM approach can be fruitful for studies of Raman spectra in systems composed of many nanoparticles, i.e., agglomerates, porous media, and nanocrystal solids.

V. DISCUSSION

In the present paper we have studied the behavior of optical phonons in contacting nonpolar nanoparticles. Basically, such phonon modes should be derived as the eigenvectors of the dynamical matrix. At the same time they obey the continuous Euclidean metric Klein-Fock-Gordon equation leading to the Laplace eigenvalue problem $\Delta \psi + q^2 \psi = 0$ with

Dirichlet boundary conditions $\psi|_{\partial \Omega} = 0$. We have used the EKFG approach as a frame and reference point, comparing its numerical solution for interpenetrating spheres with the results of a phenomenological but technically simpler method, which we called the coupled-oscillator model. We have formulated the phenomenological COM where each mode in each particle is brought into correspondence with an oscillator of a given frequency. The particle contacts cause the appearance of additional oscillator couplings proportional to the volume of particles overlaps. For not too large overlaps, the formulated algorithm describes pretty well the behavior of the levels' eigenvalues (i.e., s and p symmetric vibrational modes) as a function of particle sizes and penetration depth, being in good agreement with the original Dirichlet problem. In the case of many particles, the formulated rules do not lose their accuracy and thus the coupled-oscillator model can be used for large arrays of contacting nanoparticles. The COM approach works well for s and p levels up to the ratio of penetration depth to particle size $\delta r/R \lesssim 0.15$. At higher ratios, the complex geometry of p modes starts playing its role, and more sophisticated functions of intersection volumes are required to construct the COM Hamiltonian. However, the bands of s and p modes remain well separated for not too big scatter (when the levels of differing symmetry do not overlap). For s levels only and the noted condition on scatter size, the COM works well up to $\delta r/R < 0.5$.

To solidify our findings, we have compared the results of the COM with the yield of the microscopic dynamical matrix method for lattice vibrations. Also, the DMM has been used to consider the special but physically relevant case of faceted particles with weak van der Waals interaction. Only small frequency shifts far beyond the accuracy of the Raman spectroscopy have been obtained in this case. The interaction effects will be even weaker for spherical particles coupled by van der Waals interaction due to the lower contact surface. So the important conclusion of the present study is that Raman spectra of nanopowders can be interpreted as neglecting the effects of particle-particle contacts. In contrast, for QD nanocrystal solids and porous materials (the latter can be considered as a network of cojoined nanoparticles) the effects of the optical phonon hybridization should be strong enough to result in long-distance phonon propagation accompanied by the Raman peak shift and broadening with respect to the powder of nanoparticles of comparable size. The COM approach can be useful for their quantitative description.

It also follows from our analysis that the straightforward formulation of the perturbation theory in the spirit of a quantum-mechanics-like tight-binding model for diatomic molecules is not possible because the Dirichlet boundary conditions correspond to infinite potential barriers. Concerning the general properties of the Laplace operator eigenvalue problem, in the literature there exist only general statements like the Rayleigh-Faber-Krahn inequality [70]: The ball of the required dimension has the lowest eigenvalue when the body volume is fixed. The problems of minimization and maximization of the first Dirichlet eigenvalue for the Laplacian in the body with an obstacle [71] and minimization of the eigenvalues beyond the first one (see [72] and references therein) were also considered, but they do not help quantify the behavior of eigenvalues and eigenfunctions of intersected

spheres when varying their size mismatch and penetration parameter. Finally, the physical problem of the capacitance of joined spheres [73] also deserves to be mentioned here, but it also does not provide the required asymptotic behavior of eigenvalues for the cojoined spheres.

Inasmuch as the theory describes the behavior of the $\Delta \psi + q^2 \psi = 0$ equation eigenvalues and eigenfunctions in the manifold of the intersected spheres, our results can be applied also to *any* problem leading to this mathematical physics problem. Along with the considered case of phonons in the interpenetrating nanoparticles, the example of such a problem is the electronic level structure in quantum dot molecules (stationary Schrödinger equation). The obtained asymptotic behavior and Hamiltonian construction rules are important for the mathematical physics itself. Interestingly, the effective Hamiltonian appears to be inspired by and close to the elastic problem of coupled oscillators rather than to quantum-mechanical tight-binding-like perturbation theory.

Regarding the systems of quantum dot molecules/ nanoparticle dimers, the COM approach itself cannot provide better accuracy when considering the optical phonon modes in comparison with the DMM-BPM and EKFG approaches for it is just a sort of their approximate formulation. At the same time, it provides better comprehension of the underlying physics by drawing a parallel to the other physical systems, where similar hybridization takes place, including quantum wells with tunneling coupling and diatomic molecules. Since the formation of symmetric and antisymmetric states occurs in these systems, the COM approach gives the instructive asymptotic picture of the coupling.

One can benefit from the computational simplicity of the COM when describing large systems or if it is necessary to consider many system configurations for the purpose of averaging. The desktop-class workstations of the year 2020 can derive the phonon modes for nanoparticles containing 10 000 atoms for a time period comparable to 1 h. This number of atoms corresponds to a size of approximately 5 nm for diamond nanoparticles, which is typical for real samples [46,74–77] and is close to the theoretical prediction of the stability range of carbon nanoclusters [78]. Thus even considering computationally the dimerized diamond nanoparticles of this size becomes hardly accessible. For the case of diamond nanoparticle agglomerates containing hundreds of primary particles, porous media, or nanocrystal solids, only the COM will allow a computationally feasible approach to treat vibrational modes. Moreover, when considering disorder (the simplest case is a broadened size distribution) the problem of ensemble averaging also arises and one will again profit from the computational simplicity of the COM. An example of such a profit for the case of the ensemble of nanoparticle dimers is shown in Fig. 10. It is noteworthy that even the system size accessible by the continuous EKFG method is restricted as

well, because the mesh should be comparable to the lattice constant in order to reach the appropriate accuracy (the mesh effects will manifest most profoundly in the regions of particle contacts).

The developed theory is applicable beyond three dimensions. For instance, in the two-dimensional space the COM-like Hamiltonian can be constructed for the polariton molecules [79] and graphene [79–81], which is important to account for problems such as engineering the effective gauge fields in such structures [82]. However, in lower dimensions, due to the higher fraction of the wave function exposed to the overlap area, the dependences of matrix elements on the penetration length and overlap volume can be more complex.

VI. CONCLUSION

We have considered the problem of optical phonons and Raman spectra in the cojoined crystalline nanoparticles and coupled by weak van der Waals interaction faceted crystalline nanoparticles. In the latter case, the effects of the interaction on optical phonon modes and Raman spectra are negligible with respect to the modern experimental accuracy of Raman spectra measurements. In contrast, in the case of cojoined particles with coherently oriented crystal lattices, the effects are strong. The behavior of optical phonon modes is similar to the system of coupled harmonic oscillators with the formation of symmetric and antisymmetric wave functions. The corresponding 2×2 coupled-oscillator model Hamiltonian formulation was proposed with the terms calculated via the nanoparticle volumes and penetration lengths and demonstrated a quantitative level of accuracy. As long as the optical phonon modes obey the Euclidean metric Klein-Fock-Gordon equation and thus $\Delta \psi + q^2 \psi = 0$ in the stationary case, the COM approach can be used for any physical or mathematical physics problem leading to this equation in the manifold of cojoined spheres and could be considered as a main yield of the present study and its physical insight is threefold: drawing the parallel between the physical problem of optical phonons in nanoparticle dimers and other similar problems such as diatomic molecules and coupled quantum wells, giving the approximate solution for the $\Delta \psi + q^2 \psi = 0$ equation eigenfunction problem in the manifold of cojoined spheres and zero boundary conditions, and calculating Raman spectra of large arrays of coupled nanoparticles not accessible by other methods such as the DMM-BPM approach.

[1] G. Gouadec and P. Colomban, Raman spectroscopy of nanomaterials: How spectra relate to disorder, particle size and mechanical properties, Prog. Cryst. Growth Charact. Mater. **53**, 1 (2007).

[2] H. K. Yadav, V. Gupta, K. Sreenivas, S. P. Singh, B. Sundarakannan, and R. S. Katiyar, Low Frequency Raman Scattering from Acoustic Phonons Confined in ZnO Nanoparticles, Phys. Rev. Lett. **97**, 085502 (2006).

[3] A. K. Arora, M. Rajalakshmi, T. Ravindran, and V. Sivasubramanian, Raman spectroscopy of optical phonon confinement in nanostructured materials, J. Raman Spectrosc. **38**, 604 (2007).

[4] V. Dzhagan, M. Y. Valakh, A. Raevskaya, A. Stroyuk, S. Y. Kuchmiy, and D. Zahn, Resonant raman scattering study of cdse nanocrystals passivated with CdS and ZnS, Nanotechnology **18**, 285701 (2007).

[5] V. Dzhagan, M. Y. Valakh, O. Raevska, O. Stroyuk, S. Y. Kuchmiy, and D. Zahn, The influence of shell parameters on phonons in core-shell nanoparticles: A resonant Raman study, Nanotechnology **20**, 365704 (2009).

[6] R. Dietz, G. Parisot, and A. Meixner, Infrared absorption and Raman scattering by two-magnon processes in NiO, Phys. Rev. B **4**, 2302 (1971).

[7] T. Martin, R. Merlin, D. Huffman, and M. Cardona, Resonant two magnon Raman scattering in α-Fe_2O_3, Solid State Commun. **22**, 565 (1977).

[8] M. N. Iliev, A. P. Litvinchuk, V. G. Hadjiev, M. M. Gospodinov, V. Skumryev, and E. Ressouche, Phonon and magnon scattering of antiferromagnetic $Bi_2Fe_4O_9$, Phys. Rev. B **81**, 024302 (2010).

[9] J. E. Zucker, A. Pinczuk, D. S. Chemla, and A. C. Gossard, Resonant Raman study of low-temperature exciton localization in GaAs quantum wells, Phys. Rev. B **35**, 2892 (1987).

[10] M. Brewster, O. Schimek, S. Reich, and S. Gradečak, Exciton-phonon coupling in individual GaAs nanowires studied using resonant raman spectroscopy, Phys. Rev. B **80**, 201314(R) (2009).

[11] N. Surovtsev, I. Kupriyanov, V. Malinovsky, V. Gusev, and Y. N. Pal'yanov, Effect of nitrogen impurities on the Raman line width in diamonds, J. Phys.: Condens. Matter **11**, 4767 (1999).

[12] N. V. Surovtsev and I. N. Kupriyanov, Effect of nitrogen impurities on the Raman line width in diamond, revisited, Crystals **7**, 239 (2017).

[13] A. Y. Vinogradov, S. Grudinkin, N. Besedina, S. Koniakhin, M. Rabchinskii, E. Eidelman, and V. Golubev, Structure and properties of thin graphite-like films produced by magnetron-assisted sputtering, Semiconductors **52**, 914 (2018).

[14] A. C. Ferrari and J. Robertson, Raman spectroscopy of amorphous, nanostructured, diamond-like carbon, and nanodiamond, Philos. Trans. R. Soc. London A **362**, 2477 (2004).

[15] O. S. Kudryavtsev, R. H. Bagramov, D. G. Pasternak, A. M. Satanin, O. I. Lebedev, V. P. Filonenko, and I. I. Vlasov, Raman fingerprints of ultrasmall nanodiamonds produced from adamantane, Diam. Relat. Mater. **133**, 109770 (2023).

[16] V. I. Korepanov, H.-o. Hamaguchi, E. Osawa, V. Ermolenkov, I. K. Lednev, B. J. Etzold, O. Levinson, B. Zousman, C. P. Epperla, and H.-C. Chang, Carbon structure in nanodiamonds elucidated from Raman spectroscopy, Carbon **121**, 322 (2017).

[17] Y. Gao and P. Yin, Determination of crystallite size of nanodiamond by raman spectroscopy, Diam. Relat. Mater. **99**, 107524 (2019).

[18] V. Sachkov and V. Volodin, Localization of optical phonons in diamond nanocrystals, J. Exp. Theor. Phys. **129**, 816 (2019).

[19] S. Stehlik, M. Varga, M. Ledinsky, V. Jirasek, A. Artemenko, H. Kozak, L. Ondic, V. Skalakova, G. Argentero, T. Pennycook *et al.*, Size and purity control of HPHT nanodiamonds down to 1 nm, J. Phys. Chem. C **119**, 27708 (2015).

[20] S. Stehlik, M. Varga, M. Ledinsky, D. Miliaieva, H. Kozak, V. Skalakova, C. Mangler, T. J. Pennycook, J. C. Meyer, A. Kromka *et al.*, High-yield fabrication and properties of 1.4 nm nanodiamonds with narrow size distribution, Sci. Rep. **6**, 38419 (2016).

[21] S. Stehlik, M. Mermoux, B. Schummer, O. Vanek, K. Kolarova, P. Stenclova, A. Vlk, M. Ledinsky, R. Pfeifer, O. Romanyuk *et al.*, Size effects on surface chemistry and Raman spectra of sub-5 nm oxidized high-pressure high-temperature and detonation nanodiamonds, J. Phys. Chem. C **125**, 5647 (2021).

[22] E. Ekimov, A. A. Shiryaev, Y. Grigoriev, A. Averin, E. Shagieva, S. Stehlik, and M. Kondrin, Size-dependent thermal stability and optical properties of ultra-small nanodiamonds synthesized under high pressure, Nanomaterials **12**, 351 (2022).

[23] A. G. Yashenkin, O. I. Utesov, and S. V. Koniakhin, Bench tests for microscopic theory of raman scattering in powders of disordered nonpolar crystals: Nanodiamonds and beyond, J. Raman Spectrosc. **52**, 1847 (2021).

[24] H. Richter, Z. Wang, and L. Ley, The one phonon raman spectrum in microcrystalline silicon, Solid State Commun. **39**, 625 (1981).

[25] I. Campbell and P. M. Fauchet, The effects of microcrystal size and shape on the one phonon raman spectra of crystalline semiconductors, Solid State Commun. **58**, 739 (1986).

[26] S. Osswald, V. N. Mochalin, M. Havel, G. Yushin, and Y. Gogotsi, Phonon confinement effects in the raman spectrum of nanodiamond, Phys. Rev. B **80**, 075419 (2009).

[27] V. Paillard, P. Puech, M. Laguna, R. Carles, B. Kohn, and F. Huisken, Improved one-phonon confinement model for an accurate size determination of silicon nanocrystals, J. Appl. Phys. **86**, 1921 (1999).

[28] G. Faraci, S. Gibilisco, P. Russo, A. R. Pennisi, and S. La Rosa, Modified Raman confinement model for Si nanocrystals, Phys. Rev. B **73**, 033307 (2006).

[29] J. Zi, K. Zhang, and X. Xie, Comparison of models for raman spectra of Si nanocrystals, Phys. Rev. B **55**, 9263 (1997).

[30] S. V. Koniakhin, O. I. Utesov, I. N. Terterov, A. V. Siklitskaya, A. G. Yashenkin, and D. Solnyshkov, Raman spectra of crystalline nanoparticles: Replacement for the phonon confinement model, J. Phys. Chem. C **122**, 19219 (2018).

[31] M. Born, K. Huang, and M. Lax, Dynamical theory of crystal lattices, Am. J. Phys. **23**, 474 (1955).

[32] D. Snoke and M. Cardona, A bond polarizability model for the C_{60} Raman spectrum, Solid State Commun. **87**, 121 (1993).

[33] W. Cheng and S.-F. Ren, Calculations on the size effects of Raman intensities of silicon quantum dots, Phys. Rev. B **65**, 205305 (2002).

[34] O. I. Utesov, A. G. Yashenkin, and S. V. Koniakhin, Raman spectra of nonpolar crystalline nanoparticles: Elasticity theory-like approach for optical phonons, J. Phys. Chem. C **122**, 22738 (2018).

[35] O. I. Utesov, A. G. Yashenkin, and S. V. Koniakhin, Lifetimes of confined optical phonons and the shape of a Raman peak in disordered nanoparticles. I. Analytical treatment, Phys. Rev. B **102**, 205421 (2020).

[36] S. V. Koniakhin, O. I. Utesov, and A. G. Yashenkin, Lifetimes of confined optical phonons and the shape of a Raman peak in disordered nanoparticles. II. Numerical treatment, Phys. Rev. B **102**, 205422 (2020).

[37] O. I. Utesov, S. V. Koniakhin, and A. G. Yashenkin, Effects of bond disorder and surface amorphization on optical phonon lifetimes and Raman peak shape in crystalline nanoparticles, J. Phys. Chem. C **125**, 18444 (2021).

[38] K. C. Hass, M. A. Tamor, T. R. Anthony, and W. F. Banholzer, Lattice dynamics and Raman spectra of isotopically mixed diamond, Phys. Rev. B **45**, 7171 (1992).

[39] J. Spitzer, P. Etchegoin, M. Cardona, T. Anthony, and W. Banholzer, Isotopic-disorder induced Raman scattering in diamond, Solid State Commun. **88**, 509 (1993).

[40] H. Hanzawa, N. Umemura, Y. Nisida, H. Kanda, M. Okada, and M. Kobayashi, Disorder effects of nitrogen impurities, irradiation-induced defects, and ^{13}C isotope composition on the raman spectrum in synthetic Ib diamond, Phys. Rev. B **54**, 3793 (1996).

[41] O. Poklonskaya, S. Vyrko, A. Khomich, A. Averin, A. Khomich, R. Khmelnitsky, and N. Poklonskia, Raman scattering in natural diamond crystals implanted with high-energy ions and irradiated with fast neutrons, J. Appl. Spectrosc. **81**, 969 (2015).

[42] Y. E. Panfil, D. Shamalia, J. Cui, S. Koley, and U. Banin, Electronic coupling in colloidal quantum dot molecules; the case of CdSe/CdS core/shell homodimers, J. Chem. Phys. **151**, 224501 (2019).

[43] J. Cui, Y. E. Panfil, S. Koley, D. Shamalia, N. Waiskopf, S. Remennik, I. Popov, M. Oded, and U. Banin, Colloidal quantum dot molecules manifesting quantum coupling at room temperature, Nat. Commun. **10**, 5401 (2019).

[44] J. Cui, S. Koley, Y. E. Panfil, A. Levi, Y. Ossia, N. Waiskopf, S. Remennik, M. Oded, and U. Banin, Neck barrier engineering in quantum dot dimer molecules via intraparticle ripening, J. Am. Chem. Soc. **143**, 19816 (2021).

[45] J. Cui, S. Koley, Y. E. Panfil, A. Levi, N. Waiskopf, S. Remennik, M. Oded, and U. Banin, Semiconductor bow-tie nanoantenna from coupled colloidal quantum dot molecules, Angew. Chem. Int. Ed. **60**, 14467 (2021).

[46] A. Dideikin, A. Aleksenskii, M. Baidakova, P. Brunkov, M. Brzhezinskaya, V. Y. Davydov, V. Levitskii, S. Kidalov, Y. A. Kukushkina, D. Kirilenko *et al.*, Rehybridization of carbon on facets of detonation diamond nanocrystals and forming hydrosols of individual particles, Carbon **122**, 737 (2017).

[47] O. V. Lebedev, T. S. Kurkin, E. K. Golubev, A. L. Vasiliev, A. K. Gatin, G. P. Goncharuk, and A. N. Ozerin, Detonation synthesis nanodiamond soot as a promising filler for polymer composites, C **8**, 69 (2022).

[48] Q. Zhao, G. Gouget, J. Guo, S. Yang, T. Zhao, D. B. Straus, C. Qian, N. Oh, H. Wang, C. B. Murray *et al.*, Enhanced carrier transport in strongly coupled, epitaxially fused CdSe nanocrystal solids, Nano Lett. **21**, 3318 (2021).

[49] M. Yang, D. Huang, P. Hao, F. Zhang, X. Hou, and X. Wang, Study of the Raman peak shift and the linewidth of light-emitting porous silicon, J. Appl. Phys. **75**, 651 (1994).

[50] P. Alfaro-Calderón, M. Cruz-Irisson, and C. Wang-Chen, Theory of Raman scattering by phonons in germanium nanostructures, Nanoscale Res. Lett. **3**, 55 (2008).

[51] P. Alfaro, R. Cisneros, M. Bizarro, M. Cruz-Irisson, and C. Wang, Raman scattering by confined optical phonons in Si and Ge nanostructures, Nanoscale **3**, 1246 (2011).

[52] M. Kosović, O. Gamulin, M. Balarin, M. Ivanda, V. Ðerek, D. Ristić, M. Marciuš, and M. Ristić, Phonon confinement effects in Raman spectra of porous silicon at non-resonant excitation condition, J. Raman Spectrosc. **45**, 470 (2014).

[53] V. Valtchev and L. Tosheva, Porous nanosized particles: Preparation, properties, and applications, Chem. Rev. **113**, 6734 (2013).

[54] R. Fuchs and K. Kliewer, Optical modes of vibration in an ionic crystal slab, Phys. Rev. **140**, A2076 (1965).

[55] D. Langbein, Normal modes at small cubes and rectangular particles, J. Phys. A: Math. Gen. **9**, 627 (1976).

[56] H. Lourenço-Martins and M. Kociak, Vibrational Surface Electron-Energy-Loss Spectroscopy Probes Confined Surface-Phonon Modes, Phys. Rev. X **7**, 041059 (2017).

[57] S. Chuang and B. Do, Electron states in two coupled quantum wells—A strong coupling-of-modes approach, J. Appl. Phys. **62**, 1290 (1987).

[58] T. Jenkins and J. Lewis, A Raman study of adamantane ($C_{10}H_{16}$), diamantane ($C_{14}H_{20}$) and triamantane ($C_{18}H_{24}$) between 10 K and room temperatures, Spectrochim. Acta A **36**, 259 (1980).

[59] J. Filik, J. N. Harvey, N. L. Allan, P. W. May, J. E. Dahl, S. Liu, and R. M. Carlson, Raman spectroscopy of diamondoids, Spectrochim. Acta A **64**, 681 (2006).

[60] A. V. Kavokin, J. J. Baumberg, G. Malpuech, and F. P. Laussy, *Microcavities* (Oxford University Press, Oxford, 2017), Vol. 21.

[61] N. W. Ashcroft and N. D. Mermin, *Solid State Physics* (Cengage Learning, Boston, 1976).

[62] P. Keating, Effect of invariance requirements on the elastic strain energy of crystals with application to the diamond structure, Phys. Rev. **145**, 637 (1966).

[63] R. M. Martin, Elastic properties of ZnS structure semiconductors, Phys. Rev. B **1**, 4005 (1970).

[64] E. Anastassakis, A. Cantarero, and M. Cardona, Piezo-Raman measurements and anharmonic parameters in silicon and diamond, Phys. Rev. B **41**, 7529 (1990).

[65] E. Kane, Phonon spectra of diamond and zinc-blende semiconductors, Phys. Rev. B **31**, 7865 (1985).

[66] S. L. Mayo, B. D. Olafson, and W. A. Goddard, DREIDING: A generic force field for molecular simulations, J. Phys. Chem. **94**, 8897 (1990).

[67] H. Xia, Y. He, L. Wang, W. Zhang, X. Liu, X. Zhang, D. Feng, and H. E. Jackson, Phonon mode study of Si nanocrystals using micro-Raman spectroscopy, J. Appl. Phys. **78**, 6705 (1995).

[68] S. K. Gupta and P. K. Jha, Modified phonon confinement model for size dependent Raman shift and linewidth of silicon nanocrystals, Solid State Commun. **149**, 1989 (2009).

[69] V. Volodin and V. Sachkov, Improved model of optical phonon confinement in silicon nanocrystals, J. Exp. Theor. Phys. **116**, 87 (2013).

[70] A. Henrot, *Extremum Problems for Eigenvalues of Elliptic Operators* (Springer Science + Business Media, New York, 2006).

[71] A. Henrot and D. Zucco, Optimizing the first Dirichlet eigenvalue of the Laplacian with an obstacle, arXiv:1702.01307.

[72] A. Henrot, in *Nonlinear Evolution Equations and Related Topics*, edited by W. Arendt, H. Brézis, and M. Pierre (Birkhäuser, Basel, 2003), pp. 443–461.

[73] B. Felderhof and D. Palaniappan, Electrostatic capacitance of two unequal overlapping spheres and the rate of diffusion-controlled absorption, J. Appl. Phys. **86**, 6501 (1999).

[74] A. Ozerin, T. Kurkin, L. Ozerina, and V. Y. Dolmatov, X-ray diffraction study of the structure of detonation nanodiamonds, Crystallogr. Rep. **53**, 60 (2008).

[75] S. Koniakhin, I. Eliseev, I. Terterov, A. Shvidchenko, E. Eidelman, and M. Dubina, Molecular dynamics-based refinement of nanodiamond size measurements obtained with dynamic light scattering, Microfluid. Nanofluid. **18**, 1189 (2015).

[76] S. Koniakhin, N. Besedina, D. Kirilenko, A. Shvidchenko, and E. Eidelman, Ultracentrifugation for ultrafine nanodiamond fractionation, Superlatt. Microstruct. **113**, 204 (2018).

[77] S. V. Koniakhin, M. K. Rabchinskii, N. A. Besedina, L. V. Sharonova, A. V. Shvidchenko, and E. D. Eidelman, Evidence of absorption dominating over scattering in light attenuation by nanodiamonds, Phys. Rev. Res. **2**, 013316 (2020).

[78] J.-Y. Raty and G. Galli, Ultradispersity of diamond at the nanoscale, Nat. Mater. **2**, 792 (2003).

[79] V. G. Sala, D. D. Solnyshkov, I. Carusotto, T. Jacqmin, A. Lemaître, H. Terças, A. Nalitov, M. Abbarchi, E. Galopin, I. Sagnes, J. Bloch, G. Malpuech, and A. Amo, Spin-Orbit Coupling for Photons and Polaritons in Microstructures, Phys. Rev. X **5**, 011034 (2015).

[80] A. V. Nalitov, G. Malpuech, H. Tercas, and D. D. Solnyshkov, Spin-Orbit Coupling and the Optical Spin Hall Effect in Photonic Graphene, Phys. Rev. Lett. **114**, 026803 (2015).

[81] A. V. Nalitov, D. D. Solnyshkov, and G. Malpuech, Polariton $\mathbb{Z}$ Topological Insulator, Phys. Rev. Lett. **114**, 116401 (2015).

[82] O. Jamadi, E. Rozas, G. Salerno, M. Milićević, T. Ozawa, I. Sagnes, A. Lemaître, L. Le Gratiet, A. Harouri, I. Carusotto *et al.*, Direct observation of photonic Landau levels and helical edge states in strained honeycomb lattices, Light Sci. Appl. **9**, 144 (2020).